Epithelial control of colonisation by *Streptococcus pneumoniae* at the human mucosal surface

Caroline M Weight[1], Cristina Venturini[1], Sherin Pojar[2], Simon P. Jochems[2], Jesús Reiné[2], Elissavet Nikolaou[2], Carla Solórzano[2], Mahdad Noursadeghi[1], Jeremy S Brown[3], Daniela M. Ferreira[2], Robert S Heyderman[1]

[1]Division of Infection and Immunity, University College London, London, United Kingdom, [2]Department of Clinical Sciences, Liverpool School of Tropical Medicine, Liverpool, United Kingdom, [3]Department of Respiratory Medicine, University College London, London, United Kingdom

Corresponding Author: Dr Caroline M. Weight, Division of Infection and Immunity, The Rayne Building, 5 University Street, University College London, WC1E 6JF, UK.

Email: c.weight@ucl.ac.uk; Tel: +44 20 3108 2351

ABSTRACT

Control of *Streptococcus pneumoniae* colonisation at human mucosal surfaces is critical to reducing the burden of pneumonia and invasive pneumococcal disease, interrupting transmission, and achieving herd protection. Using an Experimental Human Pneumococcal Carriage Model (EHPC), we show that *S. pneumoniae* colonisation is associated with epithelial surface adherence, microcolony formation and invasion, without overt disease. The finding of co-association with junctional proteins (JAM-A and β catenin) provides a possible mechanism for this so-called micro-invasion. Clearance of the pneumococcus from the mucosa occurs in the context of micro-invasion. Using epithelial modules from a human epithelial cell model that recapitulates our *in vivo* findings, comprising innate signalling/ regulatory pathways, inflammatory mediators, cellular metabolism and stress response genes, we find that inflammation in the EHPC model is most prominent around the time of bacterial clearance. These results show that rather than being confined to the epithelial surface and the overlying mucus layer, the pneumococcus undergoes micro-invasion which enhances the inflammatory/ innate immune response associated with clearance which may also trigger transmission.

Introduction

Colonisation of upper respiratory tract (URT) mucosa by a range of pathogenic bacteria is a necessary precursor to both disease and onward transmission. Although *Streptococcus pneumoniae* is a common coloniser of the human nasopharynx, it is estimated to be responsible for >500,000 deaths due to pneumonia, meningitis and sepsis in children under five years of age worldwide[1].

In Europe and North America, there has been a dramatic effect of pneumococcal conjugate vaccine (PCV) on vaccine serotype (VT) invasive disease, carriage and transmission[2]. However, the emergence of non-VT pneumococcal disease worldwide and the more modest impact of PCV on colonisation in high transmission settings, threaten this success[3]. Control of pneumococcal URT colonisation in humans is not fully understood[4], and so defining the mechanistic basis for host control of pneumococcal colonisation at the mucosal surface is therefore crucial for the further optimisation of therapeutic interventions which target carriage and transmission.

Naturally acquired immunity to pneumococcal antigens is primarily mediated by mucosal T cells, anti-protein antibodies, controlled by Treg[5,6]. The URT epithelium is central to this process[7], binding and transporting antibodies, sensing bacteria via a range of surface and intracellular pathogen-associated molecular patterns (PAMPs) receptors, and rapidly transducing signals to recruit innate and inflammatory immune mechanisms[8,9].

Murine models suggest that adherence of *S. pneumoniae* to the mucosal epithelium may be followed by paracellular transmigration and tight junction modulation[10,11]. In contrast, studies of immortalised epithelial cell monolayers implicate endocytosis of *S. pneumoniae*, mediated though pneumococcal protein C–polymeric immunoglobulin receptor interactions[12,13]. The relative importance of epithelial endocytosis and paracellular migration in colonisation and invasion remains uncertain[13], but could influence epithelial sensing of this otherwise extracellular pathogen[11]. This may include TLR2 signalling via lipoteichoic acid[14,15], Nod1 signalling via peptidoglycan[16] and TLR4 signalling via

78 pneumolysin, a pore-forming toxin that induces inflammation and mediates both clearance and
79 transmission in an infant mouse model[17-19].

80

81 We have explored the hypothesis that pneumococcal-epithelial engagement dictates the
82 inflammatory/ innate immune response and therefore the outcome of colonisation. Much of what we
83 understand of the control of pneumococcal colonisation is derived from epidemiological studies and
84 murine carriage models. The experimental human pneumococcal carriage (EHPC) model provides
85 a well-controlled, reproducible tool to characterise the cellular and molecular mechanisms that
86 underlie pneumococcal colonisation in humans[20]. We have used human epithelial cell lines to further
87 probe these mechanisms and derive epithelial transcriptome module to interrogate the host response
88 in the EHPC model. We show that pneumococcal colonisation in humans is characterised by
89 microcolony formation, junctional protein association and migration across the epithelial barrier
90 without disease, which we have termed micro-invasion. This pattern of bacterial-host cell association
91 shapes epithelial sensing of *S. pneumoniae,* which is partially pneumolysin dependent. Together,
92 our data suggest that pneumococcal engagement with the epithelium in the early phases of
93 colonisation may occur without eliciting a marked host response. As colonisation becomes more
94 established, epithelial sensing of *S. pneumoniae* enhances innate immunity/ inflammation which we
95 propose promotes clearance and may trigger transmission.

96

97

98 **RESULTS**

99

100 **Pneumococcal colonisation of the human nasopharynx is associated with epithelial**
101 **adhesion, microcolony formation and micro-invasion**

102 We have used an EHPC model[21] to capture the epithelial events central to pneumococcal
103 colonisation, obtaining human mucosal samples by curette biopsy. We defined a carrier as an
104 individual colonised by 6B *S. pneumoniae* as detected by culture of nasal wash at any day following

105 inoculation. Clearance was defined as when *S. pneumoniae* colonisation became negative by culture
106 of nasal wash.
107
108 Colonisation was detected in 9/13 healthy volunteers by culture, 12/13 by microscopy and 9/11 by
109 LytA PCR (Table 1). Carriage was detected by culture/ PCR at day 2, whereas maximum detection
110 by microscopy was evident at day 6. This is not explained by colonisation density and therefore the
111 sensitivity of culture/ PCR. This could be explained by greater association with the epithelium
112 (detected by all techniques) rather than the overlying mucus (detected by culture/PCR but not
113 microscopy) over time. Clearance generally occurred between day 9 and day 27 (Table 1 and Figure
114 1b).
115
116 Curette biopsy samples visualised by confocal microscopy using Wheat Germ Agglutinin (WGA) as
117 a marker for surface carbohydrates and Junctional Adhesion Molecule A (JAM-A) as a marker of
118 tight junctions, yielded intact sheets of epithelial cells associated with polymorphonuclear leukocytes,
119 characterised morphologically (Figure 1a and Supplementary Figure 1a). Amongst carriers,
120 pneumococci were found on the epithelial surface (Table 1; Figure 1c, Figure 1d) which over time
121 became associated with microcolony formation (Figure 1e). There was evidence of pneumococcal
122 invasion of the epithelial monolayer ("micro-invasion", Figure 1e-f). Pneumococci were also
123 observed in phagocytic cells (Supplementary Figure 1a). Colonisation was frequently characterised
124 by co-association between *S. pneumoniae* and JAM-A (Figure 1f). This intimate association between
125 inoculated pneumococci and the mucosa in the EHPC model is suggestive of an active process that
126 reflects natural asymptomatic pneumococcal carriage in humans.
127
128 **Epithelial surface marker expression *in vivo* is not altered in response to colonisation with *S.***
129 ***pneumoniae***
130 To determine whether pneumococcal colonisation leads to epithelial activation, we analysed nasal
131 curette biopsy cells for surface expression of EpCAM (epithelial cell identification), IL-22Ra1,
132 HLADR, CD40, CD54 and CD107a (Supplementary Figure 2a-d). We did not detect a significant
133 change in the relative expression of IL-22Ra1 (protects the epithelial barrier, promotes anti-microbial

134 product secretion during infection, modulating pneumococcal carriage and clearance[22]), HLADR
135 (mediates T cell-antigen recognition and is a marker of epithelial activation[23]), CD40 (co-stimulatory
136 protein which binds CD154[24] (Supplementary Figure 2e-g)) or CD54 (a leukocyte adhesion molecule
137 which is also upregulated by CD40[24,25], initiating neutrophil migration and recruitment[26]) (Figure 1g).
138 However, although numbers of epithelial cells expressing CD107a did not change over time (Figure
139 1h), we observed an increase in CD107a^{high} expression at day 2 post inoculation in carriage positive
140 volunteers vs. carriage negative volunteers (Figure 1h). CD107a in the epithelium forms the
141 membrane glycoprotein of late endosomes and phagolysosomes[13] and has previously been
142 implicated in pneumococcal endocytosis[13]. These data highlight the ability of the pneumococcus to
143 colonise the nasopharynx without marked inflammation and potentially implicate CD107a in the
144 process.

145

146 ***S. pneumoniae* infection of nasopharyngeal epithelial cells *in vitro* is associated with**
147 **pneumococcal adhesion, microcolony formation and micro-invasion**

148 To further understand epithelial responses to *S. pneumoniae* observed in the EHPC model, we
149 undertook infection experiments with Detroit 562 epithelial cells. We compared the 6B response with
150 two other representative clinical isolates, TIGR4 (the original sequenced strain[27]) and 23F, and a
151 TIGR4 pneumolysin deletion mutant strain (dPly).

152

153 TIGR4 association with Detroit 562 cells was over 100-fold higher for adhesion and over 70-fold
154 higher for invasion after three hours infection, compared to 6B or 23F strains (Figure 2a-b).
155 Pneumococcal adhesion to the epithelial surface was associated with microcolony formation and
156 internalisation of this conventionally extracellular pathogen[11] (Figure 2d-e, Supplementary Figure
157 3a). Intracellular pneumococci were contained within intracellular vesicles suggestive of endocytosis,
158 which was most marked with the TIGR4 strain (Figure 2b)[13]. Intracellular pneumococci were coated
159 with JAM-A (Figure 2f, Supplementary Figure 3a) and associated with the adherens junction protein
160 β catenin but not Claudin 4 (Supplementary Figure 3a). Pneumococci were located laterally,
161 transiting between cell junctions (Figure 2g), at the level of the nuclei and below the basal membrane

162 (Figure 2h). Transmigration across the epithelium (endocytosis or paracellular movement), as
163 measured by the culture of pneumococci from the basal chamber of transwell inserts, was most
164 marked with 23F (Figure 2c, five-fold higher compared to TIGR4, after three hours infection). A
165 similar pattern of epithelial interaction was also seen at one hour suggesting these observations are
166 not simply explained by differential growth.

167

168 Epithelial infection with the dPly-TIGR4 mutant showed a significant increase in adherence (Figure
169 2a, ten-fold higher after three hours infection), internalisation (Figure 2b, three-fold higher after three
170 hours infection), but no significant differences in transmigration (Figure 2c) compared to the wild-
171 type strain, implicating pneumolysin in the modulation of bacterial interactions with the epithelium.

172

173 Similar patterns of adherence and invasion were observed in infection experiments with human
174 Calu3 and A549 epithelial cells demonstrating that these findings are cell-line independent
175 (Supplementary Figure 4). Furthermore, primary epithelial cells differentiated on an air-liquid
176 interface for 30 days and co-cultured with either 6B or 23F *S. pneumoniae* also revealed
177 pneumococcal microcolony formation, micro-invasion and epithelial junctional protein association
178 (Supplementary Figure 1b).

179

180 Together these data show the strain dependency of pneumococcal-epithelial interactions *in vitro*
181 which mirror the pathways for epithelial micro-invasion seen *in vivo*.

182

183 **Endocytosis-related micro-invasion and transmigration**

184 To confirm that the pneumococcal endocytosis leads to transmigration across the epithelium,
185 endocytosis was inhibited with dynasore and nystatin[13]. After one hour of infection, cellular uptake
186 of 23F was inhibited by 82% (Figure 2i) and transmigration across the cell monolayer by 85% (Figure
187 2j). This inhibition of endocytosis and transmigration was also seen with TIGR4 (data not shown). In

188 agreement with previous studies using A549 and Calu3 cells[28], we found that viable pneumococci in
189 Detroit 562 cells decreased over time (Supplementary Figure 5a). Using gentamicin treatment to
190 eliminate the original extracellular inoculum, we observed *S. pneumoniae* in the apical and basal
191 media (Supplementary Figure 5b), suggesting egress from the epithelium.

192

193 **Loss of epithelial cell barrier function is not a pre-requisite for micro-invasion by *S.***
194 ***pneumoniae***

195 *S. pneumoniae* has been shown to affect the integrity of epithelial barriers and tight junction function
196 in murine models[10,29]. Having demonstrated pneumococcal micro-invasion without obvious epithelial
197 morphological disruption, we explored possible effects on epithelial barrier function by measuring
198 trans-epithelial electrical resistance (TEER) and permeability to 4kDa FITC-dextran in Detroit 562
199 cells. TEER was not adversely affected by pneumococcal co-culture (Figure 2k) and permeability
200 was maintained with all the pneumococcal strains at three hours post-infection (Figure 2l). Although
201 co-localisation of pneumococci was seen with host proteins, we did not detect marked epithelial
202 membrane carbohydrate or protein re-distribution (WGA, Claudin 4 JAM-A, β catenin,
203 Supplementary Figure 3a). Similar observations were made with A549 cells and Calu3 cells
204 (Supplementary Figure 4). These data suggest that pneumococcal micro-invasion was not
205 dependent on loss of epithelial cell barrier function during early interactions.

206

207 ***S. pneumoniae* upregulates epithelial surface CD54 and CD107a *in vitro***

208 In a similar manner to primary cells collected from nasal curettes, we assessed Detroit 562 cell
209 surface marker expression in response to *S. pneumoniae* (Supplementary Figure 7a-c). There were
210 no significant changes in IL-22Ra1, HLADR or CD40 expression in response to 6B, 23F, TIGR4 and
211 dPly-TIGR4 strains (Supplementary Figure 7d-e). However, $CD54^{high}$ expression was significantly
212 greater in response to the TIGR4 and dPly-TIGR4 strains, compared to non-infected cells (Figure
213 3a). Epithelial CD107a was upregulated in response to the 6B, 23F and TIGR4 strains (Figure 3b),
214 but this was not seen with dPly-TIGR4. These data implicate pneumolysin in the induction of CD107a

215 but not CD54 epithelial surface expression and support the possibility that CD107a is involved in
216 pneumococcal-epithelial micro-invasion events seen *in vivo*.

217

218 **_Streptococcus pneumoniae_ induces epithelial secretion of IL-6, IL-8 and CD54**

219 To assess the inflammatory consequences of pneumococcal-epithelial infections *in vitro*, we
220 measured a cytokine panel in Detroit 562 cell supernatants following *S. pneumoniae* incubation
221 (Figure 3c). We detected a significant increase in IL-6 and IL-8, which were strain dependent and
222 partially pneumolysin dependent. In line with surface marker observations, only TIGR4 significantly
223 upregulated the secretion of soluble CD54, which was dependent on pneumolysin (Figure 3c). These
224 data highlight the less inflammatory nature of the 6B strain compared to the more invasive strain,
225 TIGR4, and the importance of pneumolysin in the epithelial response. Pneumococcal wild-type strain
226 differences were not explained by differences in pneumolysin activity, as determined by hemolysis
227 (Supplementary Figure 7).

228

229 **Innate transcriptomic response to epithelial infection by *S. pneumoniae in vitro***

230 To explore the hypothesis that the pattern of epithelial adhesion and micro-invasion results in
231 differential epithelial responses, we performed RNAseq of Detroit 562 cells infected with our panel
232 of *S. pneumoniae* strains. In comparison to non-infected epithelial cell cultures (Figure 4a), infection
233 with TIGR4 upregulated expression of 1127 genes (550 unique genes), 23F upregulated 650 genes
234 (69 unique genes), and 6B upregulated 153 genes (10 unique genes). The pneumolysin deficient
235 isogenic mutant of TIGR4 upregulated 220 genes (14 unique genes). Compared to non-infected
236 cells, 1193 genes were upregulated by *S. pneumoniae* infection overall and 93 were core to all
237 strains tested. The sets of genes upregulated by each strain individually were subjected to core and
238 interactome and pathway-enrichment analysis for functional annotation of the cellular response at
239 systems level (Figure 4b, Online Supplementary File). From 20 clusters of pathways, significant
240 enrichment of innate immune system responses was evident in all strains and included specific
241 enrichment in Toll receptor cascades, peptide ligand-binding receptors, NFkB and MAP kinase

242 activation, Interferon signalling and cytokine and chemokine signalling, (Figure 4b, 4c). In general,
243 the greater number of transcripts upregulated by TIGR4 and 23F strains compared to 6B translated
244 to a larger number of biological pathways with differential innate immune responses to each strain
245 (Figure 4b). Fewer transcriptional responses at the level of functional pathways in response to dPly-
246 TIGR4 is consistent with a role for pneumolysin in innate immune recognition of *S. pneumoniae*[30].
247 Fewer transcriptional responses to 6B is consistent with our observations that this strain exhibits the
248 lowest level of cellular association and transmigration.

249

250 To elucidate the pathways that drive the transcriptional responses to each strain, we also undertook
251 transcription factor binding site enrichment analysis (Figure 4d, Online Supplementary File). The
252 responses to 6B and pneumolysin deficient strains were principally enriched in binding sites for the
253 NFkB/Rel family of transcription factors, indicating that an NFkB activation pathway was the
254 dominant driver for responses to these strains. In contrast, cellular responses to TIGR4 and 23F
255 strains revealed enriched binding sites for more diverse transcription factors, suggesting diverse
256 molecular pathways by which these strains may influence cellular function. This analysis revealed
257 particular enrichment of binding sites for beta-beta-alpha zinc finger superfamily of transcription
258 factors, including SP1 and KLF4, suggesting that these strains upregulate mitogen activated protein
259 kinase pathways upstream of these transcription factors[31].

260

261 **Epithelial transcriptomic responses to 6B are detectable *in vivo***

262 Next, we sought to test whether these epithelial transcriptomic responses to *S. pneumoniae* were
263 also evident in the 6B EHPC model. We compared nasal transcriptomes sampled at two or nine days
264 after inoculation to pre-inoculation samples. These revealed significant enrichment of 158 transcripts
265 among individuals who became colonised (Supplementary Figure 9). These genes included Claudin
266 5 and Claudin 17, Defensin β 103A/B, Cadherin 16, Desmocollin 1 and Gap junction protein α1,
267 which suggests cytoskeletal re-organisation two days post-inoculation in carriage positive
268 individuals. At day 9 post-inoculation, innate molecules such as CCR3, matrix metalloproteinase 12

269 and MHC II molecules were enriched, suggesting innate activation. However, these gene sets were
270 not significantly enriched for any immune response pathway annotation perhaps because of the
271 statistical stringency necessary for genome-wide multiple testing and were not epithelial-specific.

272

273 Gene expression modules can successfully detect specific transcriptional programs in bulk tissue[32].
274 Therefore, as an alternative approach, we sought to target specific epithelial responses *in vivo* using
275 the *in vitro* interactome. A direct comparison of transcripts for 6B revealed FOSL-1, an AP-1
276 transcription factor subunit, to be enriched with carriage. To expand the sensitivity of the approach,
277 we evaluated the expression of two transcriptional modules in the nasal samples (Figure 5). A 'core'
278 module comprised of 16 interacting genes (Figure 5b) that were upregulated in the Detroit epithelium
279 by all the pneumococcal strains from Figure 5a, and a second 'integrated' module that comprised of
280 200 interacting genes (Figure 5c), which were upregulated in the Detroit epithelium by at least one
281 of the pneumococcal strains from Figure 5a. Among carriage negative individuals, we found no
282 increase in expression in either gene expression modules (Figure 5b-c). In contrast among the
283 individuals who became colonised, the expression of both modules, but significantly increased within
284 the integrated module (Figure 5b,5c), suggests that the prominence of responses at day nine may
285 reflect time-dependent proliferation of the 6B bacterial inoculum and the subsequent epithelial
286 interactions. These responses coincide around the time of bacterial clearance.

287

288

289 **DISCUSSION**

290 It is widely accepted that colonisation of the URT mucosa by many potentially pathogenic bacterial
291 species, involves transient association with the overlying mucus layer but that adherence to the
292 epithelial surface avoids mucus entrapment and muco-ciliary clearance[11,33]. While evading immunity,
293 bacterial replication then occurs prior to onward transmission to a new host. Even for *S. pneumoniae,*
294 the mechanisms underlying this transition from acquisition to established colonisation, and then
295 transmission and/or disease, are not well understood. By combining an EHPC model and *in vitro*

296 human cell culture systems, we show that pneumococcal colonisation leads to epithelial adherence,
297 microcolony formation and migration across the epithelial barrier without disease, which we have
298 termed micro-invasion. The finding of co-association with junctional proteins provides a possible
299 mechanism for micro-invasion. Clearance of the pneumococcus from the mucosa *in vivo* occurs in
300 the context of micro-invasion. Indeed, epithelial micro-invasion and not bacterial load *per s*e, appears
301 to dictate unique transcription factor binding site signatures, downstream cytokine, chemokine and
302 metabolic pathway enrichment (Figure 6).

303

304 The concept of mucosal micro-invasion moves us away from current models of colonisation where
305 the pneumococcus is held up at the epithelial surface and that invasion leads to disease. Our data
306 are supported by murine colonisation experiments[34,35] and the detection of pneumococcal DNA in
307 blood of otherwise healthy, colonised children[36]. In line with other cell culture and murine
308 models[10,13,34,37], we have demonstrated that pneumococcal micro-invasion occurs by endocytosis
309 through the formation of cytoplasmic vacuoles, and by paracellular transcytosis across the
310 epithelium. Micro-invasion of the epithelium may overcome the inaccessibility of PAMP receptors
311 located either at the epithelial basolateral surface or intracellularly[38,39]. We have found that at early
312 time points, micro-invasion *in vitro* is also characterised by pneumococcal co-association with JAM-
313 A and β catenin without evidence of barrier dysfunction. In murine models at later time points, TLR-
314 dependent Claudin 7 and Claudin 10 down-regulation enhanced pneumococcal translocation across
315 the epithelium has been observed[10]. While this may occur as inflammation becomes more prominent,
316 our data suggest that micro-invasion can happen without barrier disruption and that the epithelium
317 plays an active role in the regulation of these complex host-pathogen interactions[9].

318

319 The differential impact of micro-invasion on the epithelial transcriptomic response was striking with
320 considerable enrichment of multiple diverse transcription factors and signalling pathways related to
321 innate immunity with the most invasive pneumococcal strains. The interactome module highlights
322 that although enrichment of gene activation in response to all pneumococcal strains is apparent (the

323 core module), a more diverse range of epithelial gene activation occurs between strains, reflecting
324 specific host-pathogen interactions. Nasal colonisation in murine models is proinflammatory[40,41], but
325 our *in vitro* and EHPC experiments with serotype 6B suggests this is not always the case, whereby
326 pneumococcal-host cell adherence, growth, endocytosis and paracellular migration can be
327 established without a marked host response. In the EHPC, clearance occurred around the time the
328 epithelial transcriptomic response was most prominent. Weiser and colleagues argue that the
329 colonising pneumococcus induces the host response that mediates clearance, but also promotes
330 nutrient acquisition and onward transmission[11,17,42], which is supported by murine models[43] and
331 epidemiological studies of viral-coinfection[44]. The enrichment of binding sites for SP1 and KLF4
332 transcription factors seen in our *in vitro* data suggests a counter-regulatory process aimed at
333 minimising inflammation. KLF4 plays a role in barrier function, suppression of NFκB-dependent IL-8
334 secretion, regulation of IL-10 expression via TLR9-MyD88 and Yes-1, in response to *S. pneumoniae,*
335 which is partially dependent on autolysin LytA[31,45,46]. Thus, by exploiting micro-invasion, the
336 pneumococcus may carefully calibrate the host innate immune/ inflammatory response to promote
337 survival through transmission.
338

339 A range of pneumococcal PAMPs including pneumolysin, may trigger this epithelial sensing
340 process[17,47]. We found pneumolysin to be a prominent influencer of epithelial surface molecule
341 upregulation, cytokine production and transcriptomic inflammatory response *in vitro*. Mediated by
342 autolysin, the pneumococcus undergoes autolysis during stationery growth phase, resulting in
343 additional PAMPs' release including bacterial DNA. In mice, pneumococcal DNA triggers
344 inflammation through a DAI/STING/TBK1/IRF3 cascade[40,48], a response that may contribute to
345 pneumococcal clearance. In our *in vitro* transcriptomic analyses, we detected enriched activation of
346 IRF3/IFR7 in dPly-TIGR4. We suggest that in the context of micro-invasion, pneumococcal DNA
347 may act as a trigger of epithelial sensing, inducing inflammation[48].
348

349 Our findings are limited by the pneumococcal strains available for testing in the EHPC model to
350 enable direct comparisons with *in vitro* data. Nonetheless, the use of different strains *in vitro* has

351 enabled us and others[49,50] to determine the impact of different patterns of epithelial adherence and
352 invasion on the host inflammatory/ innate immune response. Our findings are also supported by *ex*
353 *vivo* primary cell cultures in an air-liquid interface derived from the EHPC, and by the EHPC itself.

354

355 In conclusion, our data implicates the novel finding of micro-invasion during pneumococcal
356 colonisation of otherwise healthy humans. Micro-invasion may influence the outcome of colonisation
357 by altering the balance between innate immunity/ inflammation-driven transmission and clearance.
358 This balance may be further modulated by the frequency of carriage events, pneumococcal strain
359 co-colonisation, viral co-infections and other environmental pressures[1,43]. The pathways critical for
360 onward pneumococcal transmission remain to be determined in humans. Our approach combining
361 *in vitro* with *in vivo* human systems offers a potentially tractable way to interrogate this question.

362

363

364 **ACKNOWLEDGEMENTS**

365 This study was funded by the Wellcome Trust (Grant 106846/Z/15/Z). DF is supported by the Medical
366 Research Council (grant MR/M011569/1), Bill and Melinda Gates Foundation (grant OPP1117728)
367 and the National Institute for Health Research (NIHR) Local Comprehensive Research Network.
368 LytA PCR was performed by Prof. D Bogaert, University of Edinburgh, UK. RNAseq library
369 preparation undertaken at either UCL through the Pathogens Genomic Unit or at the Wellcome
370 Sanger Institute, Hinxton with thanks to Carl Anderson. Confocal imaging facilities at LSTM were
371 funded by a Wellcome Trust Multi-User Equipment Grant (104936/Z/14/Z). Flow cytometric
372 acquisition was funded by a Wellcome Trust Multi-User Equipment Grant (104936/Z/14/Z).

373

374 **AUTHOR CONTRIBUTIONS**: CMW, SPJ, DMF and RSH conceived and designed the study. CMW,
375 SP, SPJ, JR, EN, CS acquired the data. CMW, CV, SPJ, MN, JSB, DMF, RSH analysed and
376 interpreted the data. CMW wrote the first draft of the manuscript. CMW, CV, SP, SPJ, JR, EN, CS,
377 MN, JSB, DMF, RSH commented on and approved the manuscript.

378

379 **COMPETING INTERESTS:** The authors declare no competing financial interests.

380

381

382 **REFERENCES**

383

384

385 1 O'Brien, K. L. *et al.* Burden of disease caused by Streptococcus pneumoniae in children younger than
386 5 years: global estimates. *Lancet* **374**, 893-902, doi:10.1016/S0140-6736(09)61204-6 (2009).
387 2 Whitney, C. G. *et al.* Decline in invasive pneumococcal disease after the introduction of protein-
388 polysaccharide conjugate vaccine. *N Engl J Med* **348**, 1737-1746, doi:10.1056/NEJMoa022823 (2003).
389 3 Hanage, W. P. *et al.* Carried pneumococci in Massachusetts children: the contribution of clonal
390 expansion and serotype switching. *Pediatr Infect Dis J* **30**, 302-308,
391 doi:10.1097/INF.0b013e318201a154 (2011).
392 4 Jochems, S. P., Weiser, J. N., Malley, R. & Ferreira, D. M. The immunological mechanisms that control
393 pneumococcal carriage. *PLoS Pathog* **13**, e1006665, doi:10.1371/journal.ppat.1006665 (2017).
394 5 Pido-Lopez, J., Kwok, W. W., Mitchell, T. J., Heyderman, R. S. & Williams, N. A. Acquisition of
395 pneumococci specific effector and regulatory Cd4+ T cells localising within human upper respiratory-
396 tract mucosal lymphoid tissue. *PLoS Pathog* **7**, e1002396, doi:10.1371/journal.ppat.1002396 (2011).
397 6 Zhang, Q. *et al.* Characterisation of regulatory T cells in nasal associated lymphoid tissue in children:
398 relationships with pneumococcal colonization. *PLoS Pathog* **7**, e1002175,
399 doi:10.1371/journal.ppat.1002175 (2011).
400 7 Ratner, A. J., Lysenko, E. S., Paul, M. N. & Weiser, J. N. Synergistic proinflammatory responses induced
401 by polymicrobial colonization of epithelial surfaces. *Proc Natl Acad Sci U S A* **102**, 3429-3434,
402 doi:10.1073/pnas.0500599102 (2005).
403 8 Eisele, N. A. & Anderson, D. M. Host Defense and the Airway Epithelium: Frontline Responses That
404 Protect against Bacterial Invasion and Pneumonia. *J Pathog* **2011**, 249802, doi:10.4061/2011/249802
405 (2011).
406 9 Whitsett, J. A. & Alenghat, T. Respiratory epithelial cells orchestrate pulmonary innate immunity. *Nat*
407 *Immunol* **16**, 27-35, doi:10.1038/ni.3045 (2015).
408 10 Clarke, T. B., Francella, N., Huegel, A. & Weiser, J. N. Invasive bacterial pathogens exploit TLR-
409 mediated downregulation of tight junction components to facilitate translocation across the
410 epithelium. *Cell Host Microbe* **9**, 404-414, doi:10.1016/j.chom.2011.04.012 (2011).
411 11 Weiser, J. N., Ferreira, D. M. & Paton, J. C. Streptococcus pneumoniae: transmission, colonization and
412 invasion. *Nat Rev Microbiol* **16**, 355-367, doi:10.1038/s41579-018-0001-8 (2018).
413 12 Agarwal, V., Asmat, T. M., Dierdorf, N. I., Hauck, C. R. & Hammerschmidt, S. Polymeric
414 immunoglobulin receptor-mediated invasion of Streptococcus pneumoniae into host cells requires a
415 coordinate signaling of SRC family of protein-tyrosine kinases, ERK, and c-Jun N-terminal kinase. *J Biol*
416 *Chem* **285**, 35615-35623, doi:10.1074/jbc.M110.172999 (2010).
417 13 Asmat, T. M., Agarwal, V., Saleh, M. & Hammerschmidt, S. Endocytosis of Streptococcus pneumoniae
418 via the polymeric immunoglobulin receptor of epithelial cells relies on clathrin and caveolin
419 dependent mechanisms. *Int J Med Microbiol* **304**, 1233-1246, doi:10.1016/j.ijmm.2014.10.001
420 (2014).
421 14 Beisswenger, C., Coyne, C. B., Shchepetov, M. & Weiser, J. N. Role of p38 MAP kinase and
422 transforming growth factor-beta signaling in transepithelial migration of invasive bacterial
423 pathogens. *J Biol Chem* **282**, 28700-28708, doi:10.1074/jbc.M703576200 (2007).
424 15 Tomlinson, G. *et al.* TLR-mediated inflammatory responses to Streptococcus pneumoniae are highly
425 dependent on surface expression of bacterial lipoproteins. *J Immunol* **193**, 3736-3745,
426 doi:10.4049/jimmunol.1401413 (2014).

427 16 Ratner, A. J., Aguilar, J. L., Shchepetov, M., Lysenko, E. S. & Weiser, J. N. Nod1 mediates cytoplasmic
428 sensing of combinations of extracellular bacteria. *Cell Microbiol* **9**, 1343-1351, doi:10.1111/j.1462-
429 5822.2006.00878.x (2007).
430 17 Zafar, M. A., Wang, Y., Hamaguchi, S. & Weiser, J. N. Host-to-Host Transmission of Streptococcus
431 pneumoniae Is Driven by Its Inflammatory Toxin, Pneumolysin. *Cell Host Microbe* **21**, 73-83,
432 doi:10.1016/j.chom.2016.12.005 (2017).
433 18 Malley, R. *et al.* Recognition of pneumolysin by Toll-like receptor 4 confers resistance to
434 pneumococcal infection. *Proc Natl Acad Sci U S A* **100**, 1966-1971 (2003).
435 19 Ratner, A. J. *et al.* Epithelial cells are sensitive detectors of bacterial pore-forming toxins. *J Biol Chem*
436 **281**, 12994-12998, doi:10.1074/jbc.M511431200 (2006).
437 20 Ferreira, D. M. *et al.* Controlled human infection and rechallenge with Streptococcus pneumoniae
438 reveals the protective efficacy of carriage in healthy adults. *Am J Respir Crit Care Med* **187**, 855-864,
439 doi:10.1164/rccm.201212-2277OC (2013).
440 21 Wright, A. K. *et al.* Human nasal challenge with Streptococcus pneumoniae is immunising in the
441 absence of carriage. *PLoS Pathog* **8**, e1002622, doi:10.1371/journal.ppat.1002622 (2012).
442 22 Trevejo-Nunez, G., Elsegeiny, W., Conboy, P., Chen, K. & Kolls, J. K. Critical Role of IL-22/IL22-RA1
443 Signaling in Pneumococcal Pneumonia. *J Immunol* **197**, 1877-1883, doi:10.4049/jimmunol.1600528
444 (2016).
445 23 Fais, S. *et al.* HLA-DR antigens on colonic epithelial cells in inflammatory bowel disease: I. Relation to
446 the state of activation of lamina propria lymphocytes and to the epithelial expression of other surface
447 markers. *Clin Exp Immunol* **68**, 605-612 (1987).
448 24 Propst, S. M., Denson, R., Rothstein, E., Estell, K. & Schwiebert, L. M. Proinflammatory and Th2-
449 derived cytokines modulate CD40-mediated expression of inflammatory mediators in airway
450 epithelia: implications for the role of epithelial CD40 in airway inflammation. *J Immunol* **165**, 2214-
451 2221 (2000).
452 25 Cagnoni, F. *et al.* CD40 on adult human airway epithelial cells: expression and proinflammatory
453 effects. *J Immunol* **172**, 3205-3214 (2004).
454 26 Frick, A. G. *et al.* Haemophilus influenzae stimulates ICAM-1 expression on respiratory epithelial cells.
455 *J Immunol* **164**, 4185-4196 (2000).
456 27 Tettelin, H. *et al.* Complete genome sequence of a virulent isolate of Streptococcus pneumoniae.
457 *Science* **293**, 498-506, doi:10.1126/science.1061217 (2001).
458 28 Asmat, T. M., Agarwal, V., Rath, S., Hildebrandt, J. P. & Hammerschmidt, S. Streptococcus
459 pneumoniae infection of host epithelial cells via polymeric immunoglobulin receptor transiently
460 induces calcium release from intracellular stores. *J Biol Chem* **286**, 17861-17869,
461 doi:10.1074/jbc.M110.212225 (2011).
462 29 Peter, A. *et al.* Localization and pneumococcal alteration of junction proteins in the human alveolar-
463 capillary compartment. *Histochem Cell Biol* **147**, 707-719, doi:10.1007/s00418-017-1551-y (2017).
464 30 Malley, R. *et al.* Recognition of pneumolysin by Toll-like receptor 4 confers resistance to
465 pneumococcal infection. *Proc Natl Acad Sci U S A* **100**, 1966-1971, doi:10.1073/pnas.0435928100
466 (2003).
467 31 Herta, T. *et al.* DNA-release by Streptococcus pneumoniae autolysin LytA induced Krueppel-like
468 factor 4 expression in macrophages. *Sci Rep* **8**, 5723, doi:10.1038/s41598-018-24152-1 (2018).
469 32 Pollara, G. *et al.* Validation of Immune Cell Modules in Multicellular Transcriptomic Data. *PLoS One*
470 **12**, e0169271, doi:10.1371/journal.pone.0169271 (2017).
471 33 Siegel, S. J. & Weiser, J. N. Mechanisms of Bacterial Colonization of the Respiratory Tract. *Annu Rev*
472 *Microbiol* **69**, 425-444, doi:10.1146/annurev-micro-091014-104209 (2015).
473 34 Mahdi, L. K., Ogunniyi, A. D., LeMessurier, K. S. & Paton, J. C. Pneumococcal virulence gene expression
474 and host cytokine profiles during pathogenesis of invasive disease. *Infect Immun* **76**, 646-657,
475 doi:10.1128/IAI.01161-07 (2008).
476 35 Briles, D. E., Novak, L., Hotomi, M., van Ginkel, F. W. & King, J. Nasal colonization with Streptococcus
477 pneumoniae includes subpopulations of surface and invasive pneumococci. *Infect Immun* **73**, 6945-
478 6951, doi:10.1128/IAI.73.10.6945-6951.2005 (2005).

479 36 Morpeth, S. C. *et al.* Detection of Pneumococcal DNA in Blood by Polymerase Chain Reaction for
480 Diagnosing Pneumococcal Pneumonia in Young Children From Low- and Middle-Income Countries.
481 *Clin Infect Dis* **64**, S347-S356, doi:10.1093/cid/cix145 (2017).
482 37 Talbot, U. M., Paton, A. W. & Paton, J. C. Uptake of Streptococcus pneumoniae by respiratory
483 epithelial cells. *Infect Immun* **64**, 3772-3777 (1996).
484 38 Gewirtz, A. T., Navas, T. A., Lyons, S., Godowski, P. J. & Madara, J. L. Cutting edge: bacterial flagellin
485 activates basolaterally expressed TLR5 to induce epithelial proinflammatory gene expression. *J*
486 *Immunol* **167**, 1882-1885 (2001).
487 39 Hornef, M. W., Wick, M. J., Rhen, M. & Normark, S. Bacterial strategies for overcoming host innate
488 and adaptive immune responses. *Nat Immunol* **3**, 1033-1040, doi:10.1038/ni1102-1033 (2002).
489 40 Koppe, U. *et al.* Streptococcus pneumoniae stimulates a STING- and IFN regulatory factor 3-
490 dependent type I IFN production in macrophages, which regulates RANTES production in
491 macrophages, cocultured alveolar epithelial cells, and mouse lungs. *J Immunol* **188**, 811-817,
492 doi:10.4049/jimmunol.1004143 (2012).
493 41 Wilson, R. *et al.* Protection against Streptococcus pneumoniae lung infection after nasopharyngeal
494 colonization requires both humoral and cellular immune responses. *Mucosal Immunol* **8**, 627-639,
495 doi:10.1038/mi.2014.95 (2015).
496 42 Zafar, M. A., Kono, M., Wang, Y., Zangari, T. & Weiser, J. N. Infant Mouse Model for the Study of
497 Shedding and Transmission during Streptococcus pneumoniae Monoinfection. *Infect Immun* **84**,
498 2714-2722, doi:10.1128/IAI.00416-16 (2016).
499 43 Plotkowski, M. C., Puchelle, E., Beck, G., Jacquot, J. & Hannoun, C. Adherence of type I Streptococcus
500 pneumoniae to tracheal epithelium of mice infected with influenza A/PR8 virus. *Am Rev Respir Dis*
501 **134**, 1040-1044, doi:10.1164/arrd.1986.134.5.1040 (1986).
502 44 Pittet, L. A., Hall-Stoodley, L., Rutkowski, M. R. & Harmsen, A. G. Influenza virus infection decreases
503 tracheal mucociliary velocity and clearance of Streptococcus pneumoniae. *Am J Respir Cell Mol Biol*
504 **42**, 450-460, doi:10.1165/rcmb.2007-0417OC (2010).
505 45 Zahlten, J. *et al.* Role of Pneumococcal Autolysin for KLF4 Expression and Chemokine Secretion in
506 Lung Epithelium. *Am J Respir Cell Mol Biol* **53**, 544-554, doi:10.1165/rcmb.2014-0024OC (2015).
507 46 Zahlten, J. *et al.* TLR9- and Src-dependent expression of Krueppel-like factor 4 controls interleukin-
508 10 expression in pneumonia. *Eur Respir J* **41**, 384-391, doi:10.1183/09031936.00196311 (2013).
509 47 Hotomi, M., Yuasa, J., Briles, D. E. & Yamanaka, N. Pneumolysin plays a key role at the initial step of
510 establishing pneumococcal nasal colonization. *Folia Microbiol (Praha)* **61**, 375-383,
511 doi:10.1007/s12223-016-0445-z (2016).
512 48 Parker, D. *et al.* Streptococcus pneumoniae DNA initiates type I interferon signaling in the respiratory
513 tract. *MBio* **2**, e00016-00011, doi:10.1128/mBio.00016-11 (2011).
514 49 Bootsma, H. J., Egmont-Petersen, M. & Hermans, P. W. Analysis of the in vitro transcriptional
515 response of human pharyngeal epithelial cells to adherent Streptococcus pneumoniae: evidence for
516 a distinct response to encapsulated strains. *Infect Immun* **75**, 5489-5499, doi:10.1128/IAI.01823-06
517 (2007).
518 50 Novick, S. *et al.* Adhesion and invasion of Streptococcus pneumoniae to primary and secondary
519 respiratory epithelial cells. *Mol Med Rep* **15**, 65-74, doi:10.3892/mmr.2016.5996 (2017).
520 51 Browall, S. *et al.* Intraclonal variations among Streptococcus pneumoniae isolates influence the
521 likelihood of invasive disease in children. *J Infect Dis* **209**, 377-388, doi:10.1093/infdis/jit481 (2014).
522 52 McCool, T. L., Cate, T. R., Moy, G. & Weiser, J. N. The immune response to pneumococcal proteins
523 during experimental human carriage. *J Exp Med* **195**, 359-365 (2002).
524 53 Hyams, C., Camberlein, E., Cohen, J. M., Bax, K. & Brown, J. S. The Streptococcus pneumoniae capsule
525 inhibits complement activity and neutrophil phagocytosis by multiple mechanisms. *Infect Immun* **78**,
526 704-715, doi:10.1128/IAI.00881-09 (2010).
527 54 Collins, A. M. *et al.* First human challenge testing of a pneumococcal vaccine. Double-blind
528 randomized controlled trial. *Am J Respir Crit Care Med* **192**, 853-858, doi:10.1164/rccm.201503-
529 0542OC (2015).

530 55 Jochems, S. P. *et al.* Novel Analysis of Immune Cells from Nasal Microbiopsy Demonstrates Reliable,
531 Reproducible Data for Immune Populations, and Superior Cytokine Detection Compared to Nasal
532 Wash. *PLoS One* **12**, e0169805, doi:10.1371/journal.pone.0169805 (2017).
533 56 Bray, N. L., Pimentel, H., Melsted, P. & Pachter, L. Near-optimal probabilistic RNA-seq quantification.
534 *Nat Biotechnol* **34**, 525-527, doi:10.1038/nbt.3519 (2016).
535 57 Soneson, C., Love, M. I. & Robinson, M. D. Differential analyses for RNA-seq: transcript-level
536 estimates improve gene-level inferences. *F1000Res* **4**, 1521, doi:10.12688/f1000research.7563.2
537 (2015).
538 58 Varet, H., Brillet-Gueguen, L., Coppee, J. Y. & Dillies, M. A. SARTools: A DESeq2- and EdgeR-Based R
539 Pipeline for Comprehensive Differential Analysis of RNA-Seq Data. *PLoS One* **11**, e0157022,
540 doi:10.1371/journal.pone.0157022 (2016).
541 59 Chakraborty, S., Datta, S. & Datta, S. Surrogate variable analysis using partial least squares (SVA-PLS)
542 in gene expression studies. *Bioinformatics* **28**, 799-806, doi:10.1093/bioinformatics/bts022 (2012).
543 60 Fang, H., Knezevic, B., Burnham, K. L. & Knight, J. C. XGR software for enhanced interpretation of
544 genomic summary data, illustrated by application to immunological traits. *Genome Med* **8**, 129,
545 doi:10.1186/s13073-016-0384-y (2016).

546

547

548 **METHODS**

549

550 **Bacteria**

551 *S. pneumoniae* clinical strains used were 6B (BHN 418[51]), 23F (P1121[52]) and TIGR4 (P1672[53]),
552 together with a pneumolysin deficient TIGR4 mutant strain (kind gift from Prof T Mitchell, University
553 of Birmingham). Stocks of bacterial aliquots grown to $O.D._{600nm}$ 0.3 were stored at -80°C, defrosted,
554 resuspended in cell culture media and used once. Colony forming units (CFU) were counted on
555 horse blood agar plates (EO Labs).

556

557 **Experimental Human Pneumococcal Carriage Model (EHPC)**

558 Following written informed consent, healthy non-smoking adults between the ages of 18 – 59 were
559 inoculated with 80,000 CFU/nostril live 6B *S. pneumoniae* (BHN418), grown to mid-log phase in
560 vegetone broth as previously described[54]. Individuals naturally colonised with *S. pneumoniae* or in
561 regular contact with at-risk individuals were excluded. Nasal washes and mucosal cells (curette
562 biopsy) from the inferior turbinate were obtained by PBS syringe and curettage using a plastic Rhino-
563 probe™ (Arlington Scientific), in this order of collection respectively, before pneumococcal
564 inoculation. Sampling was then repeated on days 2, 6, 9, and 14 - 27 post pneumococcal
565 inoculation[55]. Volunteers received the TIV vaccine intramuscularly at day 3 post pneumococcal

566 inoculation. Bacteria collected from nasal washes were quantified by CFU counts. At each time-
567 point, two curettage samples were obtained and processed for confocal immunofluorescence, flow
568 cytometry, primary cell culture and /or transcriptomic analysis by RNA sequencing (RNAseq). There
569 were no adverse events. The carriage status of each volunteer was blinded until sample analysis
570 was completed.
571 Ethical approval was given by NHS Research and Ethics Committee (REC)/Liverpool School of
572 Tropical Medicine (LSTM) REC, reference numbers: 15/NW/0146 and 14/NW/1460 and Human
573 Tissue Authority licensing number 12548.
574
575 **Human Respiratory Tract Epithelial Cell Lines**
576 Human pharyngeal carcinoma Detroit 562 epithelial cells (ATCC_CCL-138) and human bronchial
577 carcinoma Calu3 epithelial cells (ATCC_HTB-55) were grown in 10% FCS in alpha MEM media
578 (Gibco). Human alveolar epithelial carcinoma A549 epithelial cells (ATCC_CCL-185) were grown in
579 10% FCS with 1% L-glutamine in Hams/F-12 media (Gibco).
580
581 **Pneumococcal-epithelial cell co-culture**
582 *Association and Invasion assays* - confluent Detroit 562 (typically day 8 post plating), Calu3 (typically
583 day 10 post plating) and A549 (typically day 4 post plating) monolayers cultured on 12 well plates
584 (Corning), were exposed to *S. pneumoniae* for three hours in 1% FCS alpha MEM (~MOI
585 approximately 1 cell : 10 pneumococci). The medium was removed, and cells washed three times in
586 $HBSS^{+/+}$. Cells were incubated in 1% saponin for 10 minutes at 37°C and lysed by repetitive pipetting.
587 Dilutions of bacteria were plated on blood agar and colonies counted after 16 hours. To quantify
588 internalised bacteria, 100µg/ml gentamicin was added for 1 hour to the cells, which were then
589 washed another three times, before incubating with 1% Saponin and plating on blood agar plates.
590 CFUs were counted after 16 hours incubation at 37°C, 5% CO_2. There were no differences in
591 pneumococcal pre- or post-inoculum, or growth density between the strains, in the cell supernatant
592 three hours post-infection.
593

594 *Transmigration assay* - Detroit 562 cells were cultured on 3µm pore, PET Transwell Inserts
595 (ThermoFisher) typically for 10 days to achieve confluent, polarised monolayers. Calu3 cells were
596 plated onto Transwell inserts typically for 12 days and A549 cells typically for 6 days. Cell culture
597 media was changed 1 hour prior to addition of bacteria to 1% FCS (250µl apical chamber, 1ml basal
598 chamber). Resistance was recorded before and after *S. pneumoniae* were added using an EVOM2
599 (World Precision Instruments). 1mg/ml FITC-dextran (Sigma Aldrich) was added to the apical
600 chamber of selected inserts to assess permeability. Approximately 12 million bacteria were added
601 to the cells (~MOI 1 cell : 25 bacteria). During the time course, 50µl was removed, diluted and plated,
602 from the basal chamber to measure bacterial load by counting CFU/well. Permeability was recorded
603 using a FLUOstar Omega (BMG Labtech) at 488nm.
604
605 *Endocytosis inhibition assays* - Detroit 562 cells cultured on 12 well plates were treated with 100µM
606 dynasore (Cambridge Biosciences) and 7.5µg/ml nystatin (Sigma Aldrich) to block endocytosis for
607 30 minutes prior to, and for the duration of pneumococcal infection incubation period. DMSO was
608 used as a control. Cells were washed and treated with gentamicin and lysed with saponin as
609 described above.
610
611 **Confocal Microscopy**
612 For the *in vivo* analysis, mucosal cells derived by curettage from the EHPC model were placed
613 directly into 4% PFA for 1 hour. Cells were cytospun onto microscope slides and allowed to air dry.
614 For the *in vitro* analysis, epithelial cell lines on transwell membranes were fixed in either 4% PFA
615 (Pierce, Methanol Free) or 1:1 mix of methanol:acetone for 20 minutes. Cells were permeabilised
616 with 0.2% Triton X-100 for 10 minutes and blocked for 1 hour in blocking buffer (3% goat serum and
617 3% BSA in PBS) before incubation with anti-6B pneumococcal antisera, JAM-A, Claudin-4 or β-
618 catenin primary antibodies (see Supplementary Information) for one hour and then secondary and/or
619 conjugated antibodies for 45 minutes. DAPI solution was added for 5 minutes. After washing, the
620 stained samples were mounted using Aqua PolyMount (VWR International) with a coverslip onto a
621 microslide. The entire cytospin for each sample was manually viewed by microscopy for detection of
622 pneumococci. Multiple fields of view (>3) were imaged for each transwell insert, for each condition.

623 Images were captured using either an inverted LSM 700, LSM 880, or TissueFAXS Zeiss Confocal
624 Microscope. Z stacks were recorded at 1µm intervals at either 40x oil or 63x oil objectives. For the
625 *in vivo* samples, the operator (CMW) was blinded to the colonisation status of the volunteer at the
626 time of sampling.
627
628
629 **Flow cytometry**
630 For the *in vivo* analysis, cells from two curette samples were incubated in cold PBS++ (PBS
631 supplemented with 5mM EDTA and 0.5% FCS) were dislodged by pipetting and centrifuged at 440g
632 for 5 mins at 4°C. Supernatant was removed, and cells resuspended in 25µl of PBS++ with
633 Live/Dead™ Fixable Violet Dead Cell Stain (ThermoFisher). After 15 minutes incubation on ice, an
634 antibody cocktail to stain for epithelial surface marker expression (see Supplementary Information)
635 was added and incubated for another 15 minutes. Samples were vortexed, resuspended in 3.5mls
636 of PBS++ and filtered over a pre-wetted 70µm filter. Samples were transferred to a 5ml FACS tube,
637 centrifuged and resuspended in 200µl Cell Fix (BD Biosciences) and acquired on LSRII Flow
638 Cytometer (BD Biosciences). Compensation was run and applied for each experimental replicate
639 and voltages consistent throughout. Isotype controls (Biolegend) and FL-1 controls were also run for
640 each antibody. Analyses of data was performed using FlowJo LLC version 10 software. Data was
641 performed on the gated epithelial cell population and only samples containing 500 or more cells are
642 reported.
643
644 For the *in vitro* analysis, confluent monolayers of Detroit 562 cells on 6 well plates were incubated
645 with *S. pneumoniae* for 6 hours in 1% FCS phenol free alpha MEM (base media, Life Technologies).
646 Cells were washed three times in PBS and gently lifted from the plate using a cell scraper in 300µl
647 of base media supplemented with 1mM EDTA. Samples were transferred to 5ml FACS tubes and
648 placed on ice for the duration of the protocol. Each cell sample was incubated with an antibody
649 cocktail for epithelial surface marker expression (see Supplemental Information) for 30 minutes
650 before rinsing in 1ml base media and centrifuging at 300g for 5 minutes at 4°C. Cells were fixed in
651 600µl of 4% PFA and acquired on a LSR II Flow Cytometer (BD Biosciences). Compensation was

652 run and applied for each experimental replicate and voltages consistent throughout. Isotype controls
653 (BD Biosciences), FL-1 and single stains were also run for each experiment. Samples were acquired
654 until 300,000 events had been collected. Analyses were performed using FlowJo LLC version 10
655 software.
656
657
658 **ELISAs**
659 Supernatant from Detroit 562 cells that had been incubated with *S. pneumoniae* for 6 hours, was
660 collected for cytokine analysis. IL-1β, IL-6, IL-8, IFNγ, TNFα, ICAM-1 DuoSet® ELISA kits were
661 purchased from R&D Systems and protocol followed according to manufacturers' instructions.
662
663 **RNA samples and sequencing (RNASeq)**

664 Mucosal curettage samples and epithelial cell cultures (incubated with or without *S. pneumoniae* for
665 3 hours) were collected in RNALater (ThermoFisher) and stored at -80°C. RNA Extraction was
666 performed using the RNEasy micro kit (Qiagen) and genomic DNA was removed with on column
667 DNA digestion or with the Turbo DNA-free Kit (Qiagen). Extracted RNA quality was assessed and
668 quantified using a BioAnalyser (Agilent 2100). Library preparation and RNA-sequencing (Illumina
669 Hiseq4000, 20M reads, 100 paired-end reads) were performed at the Beijing Genome Institute
670 (China) or the Sanger Institute (UK) for mucosal curettage samples. For the Detroit 562 samples,
671 library preparation was performed using the Kappa Hyperprep kit (Roche Diagnostics) and
672 sequencing was performed by the Pathogens Genomic Unit (UCL) on the Illumina Nextseq using
673 the Nextseq 500/550 High Output 75 cycle kit (Illumina) according to manufacturers' instructions,
674 giving 15-20 million 41bp paired end reads per sample.

675

676 All data processing and analysis was conducted in R, language and environment for statistical
677 computing (https://www.R-project.org). Paired end reads were mapped to the Ensembl human
678 transcriptome reference sequence (homo sapiens GRCh38). Mapping and generation of read counts

679 per transcript were performed using Kallisto[56], based on pseudoalignment. R/Bioconductor package
680 Tximport was used to import the mapped counts data and summarise the transcripts-level data into
681 gene level data[57]. DESeq2 and SARTools packages[58], were used for differential gene expression
682 analysis, using a false discovery rate (FDR) <0.05, following normalisation with a negative binomial
683 generalised linear model. In addition, transcript abundance for protein coding genes was expressed
684 as log_2-transformed transcripts per million (TPM) by normalising the read counts to gene length and
685 then read depth. Transcriptomes from nasal samples ranged from 16 to 66 million reads per sample
686 and in principle component analysis, revealed a batch effect that was corrected by the Combat
687 function in the Surrogate Variable Analysis (SVA) R/Bioconductor package (Supplementary
688 Figure)[59].

689

690 Identification of interacting networks and pathway enrichment analysis was performed using XGR R
691 package[60]. Interacting genes (supported by at least one experimental source of evidence) were
692 identified from the Pathway Commons database for directed interactions (Supplementary File).
693 These were then subjected to Reactome pathway enrichment analysis with FDR<0.05
694 (Supplementary File). K-means clustering of Jaccard indices to quantify similarity between the
695 composition of genes mapping to each pathway was used to identify 20 groups of pathways, from
696 which the pathway consisting of the largest total number of genes was selected to provide a
697 representative annotation for each group. The expression of gene modules in the nasal
698 transcriptomes was represented by the mean Log_2 TPM value of the genes in each module.

699

700 **Code Availability**

701 Codes used to process the RNAseq data can be found at https://github.com/cristina86cristina.

702

703 **Statistics**

704 All experiments were conducted with replicates in three or more independent experiments unless
705 stated otherwise. Error bars represent SEM unless stated otherwise. GraphPad Prism Version 10

706 was used to perform two-tailed parametric (t-tests or ANOVA) or non-parametric (Mann-Whitney or
707 Kruskal-Wallis tests) analysis, which was based on the Shapiro-Wilk normality test. P values less
708 than 0.05 were considered significant and are derived from non-parametric statistical tests unless
709 stated otherwise.

710

711

712

713

714 **FIGURE LEGENDS**

715

716 **Table 1. *Streptococcus pneumoniae* association with the nasal epithelium in the EHPC model**
717 **detected by culture, confocal microscopy and LytA PCR**

718 Nasal washes and nasal curette biopsies were collected from carriage positive and carriage negative
719 volunteers over time. Standard methods for measuring bacterial density by culture (CFU) and LytA
720 PCR were compared against counts visualised by confocal microscopy for pneumococcal
721 association with nasal cells over time. The data was derived from 13 volunteers. + (1-10
722 pneumococci); ++ (11-50 pneumococci); +++ (51-100 pneumococci); ++++ (>100 pneumococci); n/a
723 = reading not taken.

724

725 **Figure 1. *Streptococcus pneumoniae* colonisation of the human nasal epithelium from the**
726 **EHPC model is associated with adhesion, microcolony formation and micro-invasion but**
727 **does not alter epithelial surface marker expression, in response to 6B colonisation**

728 (a) Representative fields from the EHPC model nasal curette biopsies show intact epithelium can be
729 obtained from the samples (as visualised by XY planes) and they retain their size and shape (as
730 visualised by XZ planes). Cells were stained with Wheat Germ Agglutinin (WGA) or Junctional
731 Adhesion Molecule -A (JAM-A, red) and nuclei. (b) The pattern of pneumococcal density detected
732 by culture and microscopy. (c) The proportion of bacteria located on the cell surface, intracellularly,
733 or paracellularly visualised by confocal microscopy, quantified from 8 volunteers collected over time

734 from microscopy counts. (d) Cells were stained for surface carbohydrates using WGA (red), and the
735 bacteria were marked with specific serotype antiserum (green). XY images of 1µm slices through a
736 layer of cells, with bacteria associated. (e) Examples of cells showing; (ei) Microcolony formation on
737 the surface of the epithelium, (eii) bacterial internalization, (eiii) migration through epithelial uptake
738 internally or between cells. (f) Co-association between *S. pneumoniae* (green) and JAM-A (red).
739 Nuclei (blue). Bacterial uptake appeared co-associated with JAM-A (yellow).

740 Epithelial cells from nasal curette biopsies were analysed by flow cytometry for (g) CD54 and (h)
741 CD107a. Results were expressed as median fluorescence intensity (left) and high cell surface
742 expression (≥95% of the baseline expression) representing at least two volunteers per time point
743 who were carriage negative (black) and carriage positive (grey).

744

745 **Figure 2. *Streptococcus pneumoniae* infection of nasopharyngeal epithelium *in vitro* is**
746 **associated with adhesion, microcolony formation, micro-invasion, transmigration and is**
747 **partially influenced by pneumolysin. Transmigration is endocytosis-dependent but does not**
748 **disrupt barrier function**

749 (a) Pneumococcal association and (b) internalisation: Detroit 562 cell monolayers were stimulated
750 with pneumococci for 1 or 3 hours and the quantity of associated bacteria was determined by culture
751 (CFU); n>3. (****P = <0.0001: (a) 1hr (dashed lines, ANOVA); 3hr (solid lines, Kruskall-Wallis); (b)
752 Kruskall-Wallis). (c) Pneumococcal transmigration: Cells on transwell inserts were stimulated with
753 pneumococci for 3 hours and bacterial density in the basal chamber was determined (**P = 0.0092,
754 Kruskall-Wallis). N=5. (di) Representative pneumococcal-density (green) images of cells (blue
755 nuclei). Scale bar = 20µm. n>3. (e - h) Representative images of pneumococcal localization (green)
756 from cells (red, JAM-A), illustrating: (e) differences in adherence by 6B and TIGR4; (f) internalised
757 bacteria co-localised with JAM-A with associated intracellular vesicle-like bodies (yellow); (g) lateral
758 localisation of pneumococci (XY images) with possible paracellular movement co-associated with
759 JAM-A (XZ images); (h) basal localisation of bacteria at the level of nuclei and insert pores. n=>20.
760 (i and j) Cells were treated with dynasore and nystatin for 30 minutes prior to and during incubation

761 with 23F, for 1 hour. (i) Intracellular bacteria were quantified and CFUs counted (****P = <0.0001,
762 Mann-Whitney). (j) Transmigrated bacteria after one hour were counted by CFUs (*P = 0.013 Mann-
763 Whitney). N=4. (k and l) Cells were co-infected with pneumococci for three hours on transwell inserts.
764 (k) TEER was compared before and after exposure to pneumococci. n=9. Calcium withdrawal =
765 positive control (***P = 0.0013, unpaired T-test). n=3. (l) Permeability was assessed by leak to 4kDa
766 FITC-dextran, collected from basal chamber. N=>4. ****P = <0.0001 comparing non-infected against
767 pneumococci (Kruskall-Wallis). Blank inserts = positive control (Mann-Whitney).

768

769 **Figure 3. Epithelial surface activation-marker expression and cytokine secretion is**
770 **upregulated after *S. pneumoniae* exposure**

771 (a and b) Detroit 562 cells were stimulated with *S. pneumoniae* for 6 hours and the median
772 fluorescence intensity and high-expressing cells for (a) CD54 and (b) CD107a were analysed by flow
773 cytometry. n = >3 independent experiments (**** P < 0.0001 CD107a MFI, compared to non-infected
774 cells, ANOVA. *** P = 0.0009 for MFI CD107a, TIGR4 v dPly, unpaired T-test. *** P < 0.001 CD107a
775 high expression, compared to non-infected cells, ANOVA *P = 0.028 for high expression CD107a,
776 TIGR4 vs. dPly, Mann-Whitney). (* P = 0.048 NI v TIGR4; * P = 0.0367 NI v dPly for CD54, ANOVA).

777 (c) IL-6, IL-8 and CD54 in the supernatants from Detroit 562 cells stimulated with *S. pneumoniae* for
778 6 hours, were measured by ELISA. N = 6 independent experiments with replicates. (**** P <0.0001
779 IL-6; *** P = 0.0013 CD54; **** P < 0.0001 IL-8 (Kruskall-Wallis test)).

780

781 **Figure 3. Transmigration of *S. pneumoniae* is endocytosis-dependent but does not**
782 **disrupt barrier integrity or function**

783 (a and b) Detroit 562 cells were treated with dynasore and nystatin for 30 minutes prior to and during
784 incubation with 23F, for 1 hour. (a) Intracellular bacteria were quantified using a gentamicin
785 protection assay and CFUs counted (**** P = <0.0001, Mann-Whitney Test). (b) Bacteria that had
786 transmigrated after one hour were then counted by CFUs (* P = 0.013 Mann-Whitney Test). N = 4

787 independent experiments with replicates. (c and d) Detroit 562 cells were co-infected with
788 pneumococci for three hours on transwell inserts and TEER and permeability were recorded. (c).
789 TEER was compared before and after exposure to pneumococci. n = 9 independent experiments
790 with replicates. Calcium withdrawal was used as a positive control *** P = 0.0013 (n = 3 with
791 replicates, unpaired T-test). (d) Permeability was assessed by leak to 4kDa FITC-dextran, collected
792 from the basal chamber. N = >4 independent experiments. **** P = <0.0001 comparing non-infected
793 against pneumococcal strains (Kruskall-Wallis test). Blank inserts were used as a positive control
794 (Mann-Whitney test).

795

796 **Figure 4. *Streptococcus pneumoniae* induces epithelial innate transcriptomic responses *in***
797 ***vitro* that are influenced by the pattern of epithelial adhesion and micro-invasion**

798 (a) The total number of Detroit 562 epithelial genes upregulated following exposure to 6B, 23F,
799 TIGR4 and TIGR4-dPly pneumococci, compared to non-infected samples. N = 3 independent
800 experiments with replicates. Genes with an FDR <0.05 were considered for further analysis. The
801 matrix shows intersections for the four strains, sorted by size. Dark circles in the matrix indicates
802 sets that are part of the intersection. (b) Bubble heat map showing the results of Reactome Pathway
803 Analysis for upregulated genes in each strain compared to non-infected cells. Pathways were
804 clustered in 20 groups using K-means on Jaccard index and the biggest pathway for each group
805 was selected for representative annotation of each cluster. Individual pathways within clusters are
806 shown in Supplementary Figure 8. The colour represents the log2 z-scores (a continuum from blue
807 (lowest values) and red (highest values) and the size shows the number of genes annotated to each
808 pathway. (c) Selected bubble heat map clusters representing the individual pathways within each
809 cluster from 5b. (d) Bubble heat map showing the results of transcriptional factor analysis in
810 Opossum for each strain. Transcriptional factors are ordered by family and then sorted by number
811 of genes in the database. The colour represents the log2 z-scores (a continuum from blue to red as
812 before) and the size shows the number of genes annotated to the particular pathway.

813

814 **Figure 5. Epithelial transcriptomic responses to *Streptococcus pneumoniae* in the EHPC**
815 **model**

816 (a) Network representation generated from the *in vitro* analyses for each strain. From the genes
817 present in the networks, an integrated gene list (200 genes) and a core genes list (16 genes) were
818 generated and tested as modules in the *in vivo* data. (b and c) Upregulated genes in comparison to
819 the transcriptomes of carriage negative and carriage positive volunteers were compared between
820 time points. Plots represent log2 TPM arithmetic mean for genes in the core (b) and integrated (c)
821 modules. P = <0.05, (one tail Mann-Whitney test). Number of samples for carriage negative and
822 positive, respectively: pre (17:14), day 2 (15:14), day 9 (7:7).

823

824 **Figure 6. Model of the control of pneumococcal colonisation by the human mucosal**
825 **epithelium.**

826 Following pneumococcal adhesion and microcolony formation on the epithelial surface, the
827 host response is dependent on the subsequent pattern of interaction. Micro-invasion
828 (endocytosis and paracellular transmigration) amplifies epithelial sensing and inflammation/
829 innate immunity, which we postulate leads to immune cell engagement. This process of
830 epithelial sensing inflammation/ innate immunity may enhance both transmission and
831 clearance. Co-association with junctional proteins may facilitate migration across the barrier.

832

Table 1

		Sample day					Pneumococcal association		
ID	**Pneumococcal density**	**Pre**	**D2**	**D6**	**D9**	**D27**	**Surface**	**Intracellular**	**Lateral**
1	**Culture (CFU/ml)**	0	373	520	10	2			
	Microscopy (counts)	0	+	+	0	+	+	0	0
	LytA PCR	NEG	POS	POS	n/a	POS			
2	**Culture (CFU/ml)**	0	0	0	0	0			
	Microscopy (counts)	+	+	0	0	0	++	+	0
	LytA PCR	NEG	NEG	NEG	n/a	NEG			
3	**Culture (CFU/ml)**	0	0	0	0	0			
	Microscopy (counts)	0	+	0	0	0	+	0	0
	LytA PCR	NEG	POS	NEG	n/a	NEG			
4	**Culture (CFU/ml)**	0	3	9	0	0			
	Microscopy (counts)	0	0	0	+	0	+	0	0
	LytA PCR	NEG	POS	POS	n/a	NEG			
5	**Culture (CFU/ml)**	0	$7x10^3$	223	22	0			
	Microscopy (counts)	0	+	+	+	0	+	+	0
	LytA PCR	n/a	n/a	n/a	n/a	n/a			
6	**Culture (CFU/ml)**	0	$1.9x10^4$	$5.7x10^3$	$3.7x10^4$	11			
	Microscopy (counts)	0	++	++++	++	0	+++	++	+
	LytA PCR	NEG	POS	POS	n/a	POS			
7	**Culture (CFU/ml)**	0	822	$1.1x10^3$	160	0			
	Microscopy (counts)	0	+	+++	++	0	++	+	+
	LytA PCR	NEG	POS	POS	n/a	NEG			
8	**Culture (CFU/ml)**	0	0	0	0	0			
	Microscopy (counts)	0	0	0	0	0	0	0	0
	LytA PCR	n/a	n/a	n/a	n/a	n/a			
9	**Culture (CFU/ml)**	0	221	695	4	<1			
	Microscopy (counts)	n/a	+	+++	+	n/a	+++	+	+
	LytA PCR	NEG	POS	POS	n/a	NEG			
10	**Culture (CFU/ml)**	0	$1x10^3$	0	0	0			
	Microscopy (counts)	n/a	0	+	0	n/a	+	0	0
	LytA PCR	NEG	POS	POS	n/a	POS			
11	**Culture (CFU/ml)**	0	$1.8x10^6$	$1.8x10^6$	$1.9x10^4$	<1			
	Microscopy (counts)	n/a	++++	++++	+	n/a	+++	+	+
	LytA PCR	NEG	POS	POS	n/a	NEG			
12	**Culture (CFU/ml)**	0	0	0	0	0			
	Microscopy (counts)	NR	++	0	0	n/a	++	+	+
	LytA PCR	NEG	NEG	NEG	n/a	NEG			
13	**Culture (CFU/ml)**	0	23	2	0	0			
	Microscopy (counts)	n/a	+	0	0	n/a	+	0	0
	LytA PCR	POS	POS	POS	n/a	POS			

Figure 1

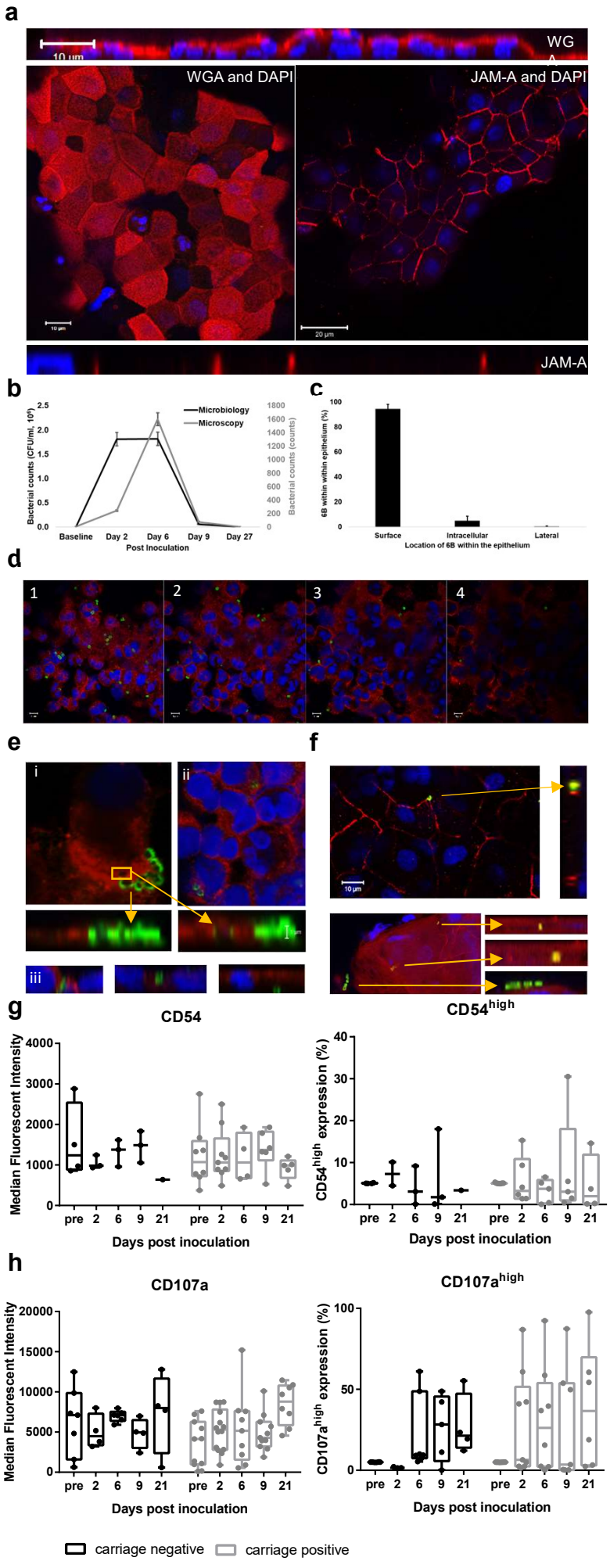
a
WG
WGA and DAPI
JAM-A and DAPI
JAM-A
b
Microbiology
Microscopy
Bacterial counts (CFU/ml, 10^6)
Bacterial counts (counts)
Baseline
Day 2
Day 6
Day 9
Day 27
Post inoculation
c
6B within within epithelium (%)
Surface
Intracellular
Lateral
Location of 6B within the epithelium
d
1
2
3
4
e
i
ii
iii
f
g
CD54
CD54high
Median Fluorescent Intensity
CD54high expression (%)
pre
Days post inoculation
h
CD107a
CD107ahigh
Median Fluorescent Intensity
CD107ahigh expression (%)
carriage negative
carriage positive

Figure 2

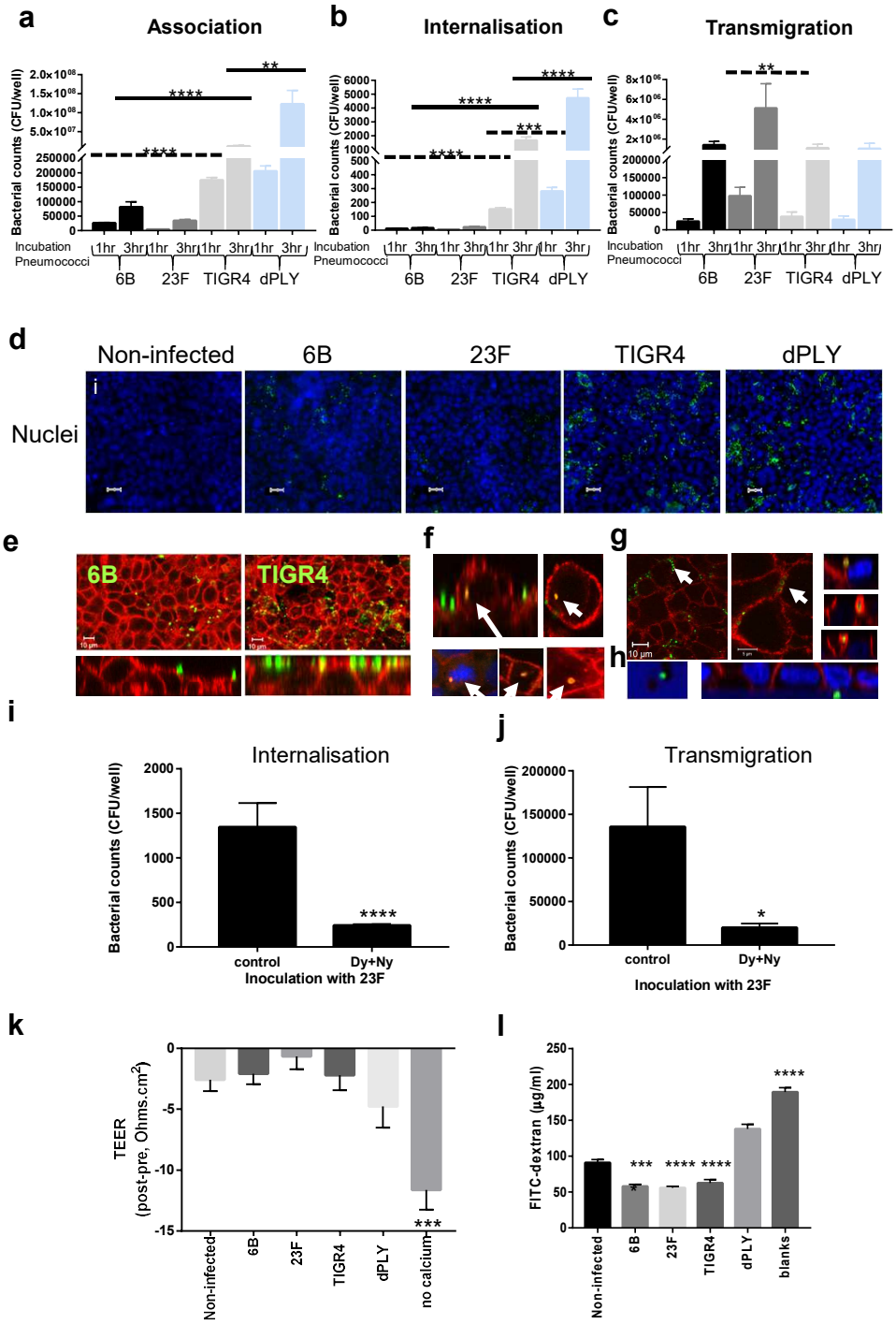
a
Association
b
Internalisation
c
Transmigration
Bacterial counts (CFU/well)
Incubation
Pneumococci
1hr 3hr 1hr 3hr 1hr 3hr 1hr 3hr
6B 23F TIGR4 dPLY
d
Non-infected
6B
23F
TIGR4
dPLY
Nuclei
e
6B
TIGR4
f
g
h
i
Internalisation
Bacterial counts (CFU/well)
control
Dy+Ny
Inoculation with 23F
j
Transmigration
Bacterial counts (CFU/well)
control
Dy+Ny
Inoculation with 23F
k
TEER
(post-pre, Ohms.cm2)
Non-infected
6B
23F
TIGR4
dPLY
no calcium
l
FITC-dextran (µg/ml)
Non-infected
6B
23F
TIGR4
dPLY
blanks

Figure 3

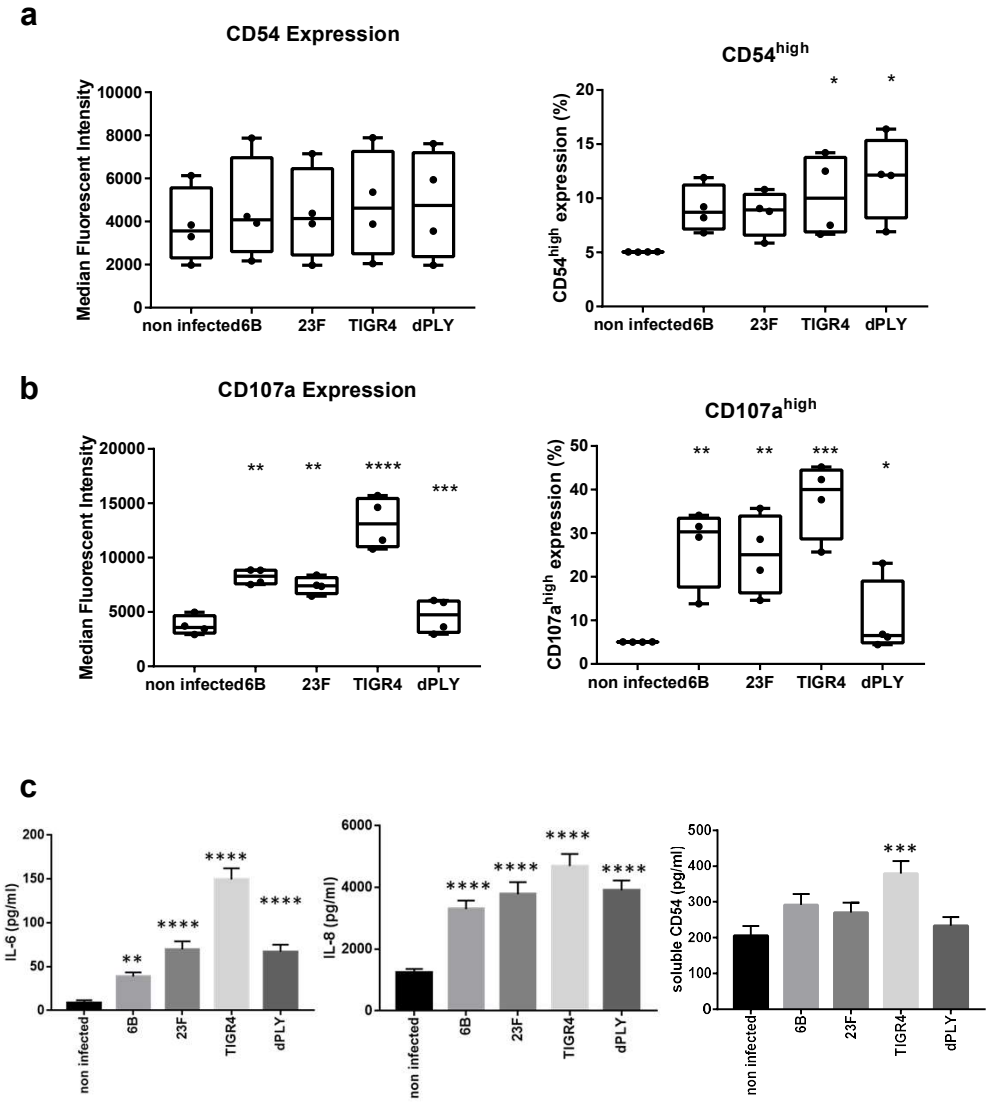
a
CD54 Expression
Median Fluorescent Intensity
10000
8000
6000
4000
2000
0
non infected
6B
23F
TIGR4
dPLY
CD54high
CD54high expression (%)
20
15
10
5
0
*
*
b
CD107a Expression
Median Fluorescent Intensity
20000
15000
10000
5000
0
**
**
****
***
CD107ahigh
CD107ahigh expression (%)
50
40
30
20
10
0
**
**
***
*
c
IL-6 (pg/ml)
200
150
100
50
0
**
****
****
****
non infected
6B
23F
TIGR4
dPLY
IL-8 (pg/ml)
6000
4000
2000
0
****
****
****
****
soluble CD54 (pg/ml)
500
400
300
200
100
0
***

Figure 4

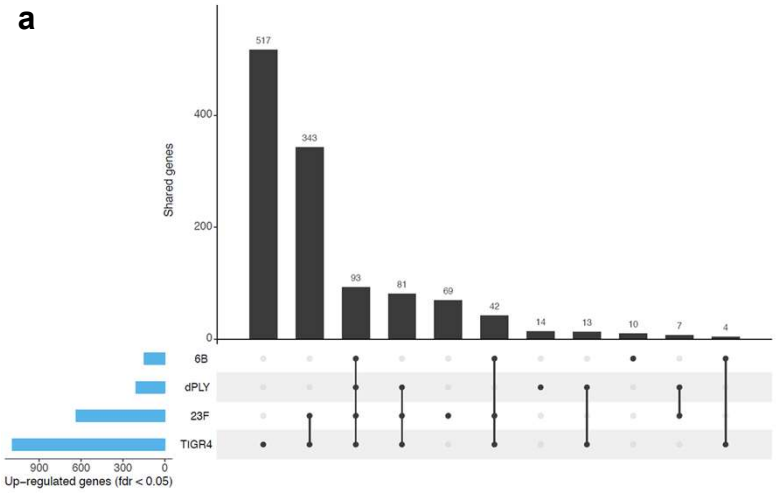
a
Shared genes
517
343
93
81
69
42
14
13
10
7
4
6B
dPLY
23F
TIGR4
Up-regulated genes (fdr < 0.05)

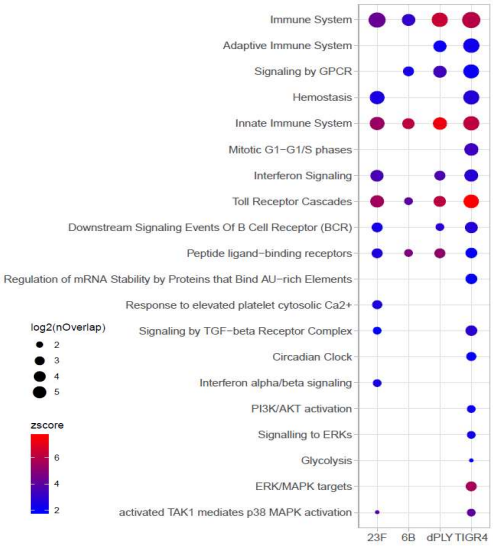
b
Immune System
Adaptive Immune System
Signaling by GPCR
Hemostasis
Innate Immune System
Mitotic G1-G1/S phases
Interferon Signaling
Toll Receptor Cascades
Downstream Signaling Events Of B Cell Receptor (BCR)
Peptide ligand-binding receptors
Regulation of mRNA Stability by Proteins that Bind AU-rich Elements
Response to elevated platelet cytosolic Ca2+
Signaling by TGF-beta Receptor Complex
Circadian Clock
Interferon alpha/beta signaling
PI3K/AKT activation
Signalling to ERKs
Glycolysis
ERK/MAPK targets
activated TAK1 mediates p38 MAPK activation
log2(nOverlap)
zscore
23F
6B
dPLY
TIGR4

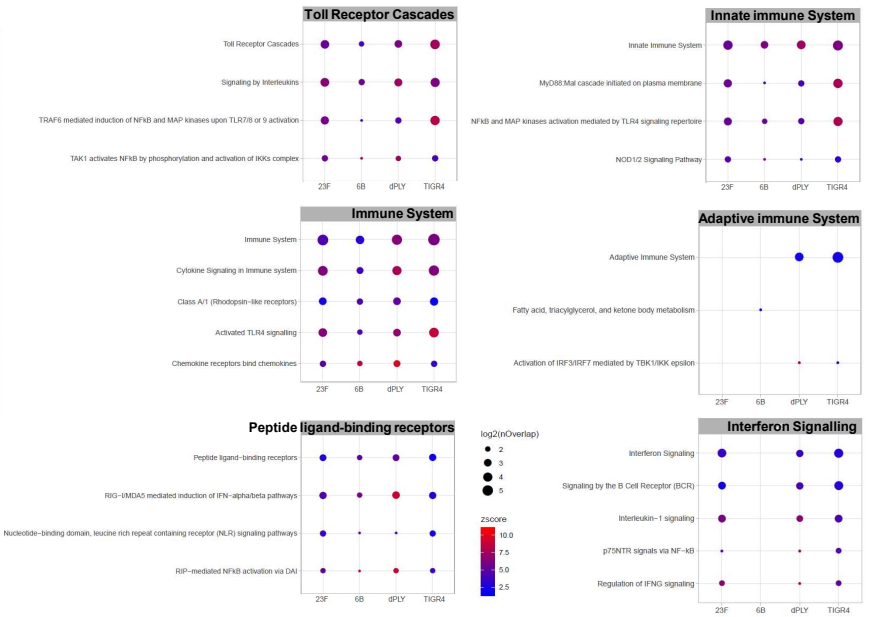
c
Toll Receptor Cascades
Toll Receptor Cascades
Signaling by Interleukins
TRAF6 mediated induction of NFkB and MAP kinases upon TLR7/8 or 9 activation
TAK1 activates NFkB by phosphorylation and activation of IKKs complex
Innate immune System
Innate Immune System
MyD88:Mal cascade initiated on plasma membrane
NFkB and MAP kinases activation mediated by TLR4 signaling repertoire
NOD1/2 Signaling Pathway
Immune System
Immune System
Cytokine Signaling in Immune system
Class A/1 (Rhodopsin-like receptors)
Activated TLR4 signalling
Chemokine receptors bind chemokines
Adaptive immune System
Adaptive Immune System
Fatty acid, triacylglycerol, and ketone body metabolism
Activation of IRF3/IRF7 mediated by TBK1/IKK epsilon
Peptide ligand-binding receptors
Peptide ligand-binding receptors
RIG-I/MDA5 mediated induction of IFN-alpha/beta pathways
Nucleotide-binding domain, leucine rich repeat containing receptor (NLR) signaling pathways
RIP-mediated NFkB activation via DAI
Interferon Signalling
Interferon Signaling
Signaling by the B Cell Receptor (BCR)
Interleukin-1 signaling
p75NTR signals via NF-kB
Regulation of IFNG signaling
log2(nOverlap)
zscore
23F
6B
dPLY
TIGR4

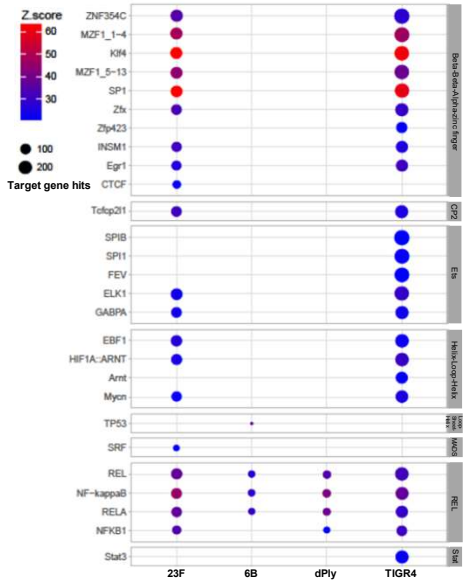
d
Z.score
Target gene hits
ZNF354C
MZF1_1-4
Klf4
MZF1_5-13
SP1
Zfx
Zfp423
INSM1
Egr1
CTCF
Tcfcp2l1
SPIB
SPI1
FEV
ELK1
GABPA
EBF1
HIF1A::ARNT
Arnt
Mycn
TP53
SRF
REL
NF-kappaB
RELA
NFKB1
Stat3
23F
6B
dPly
TIGR4

Figure 5

a

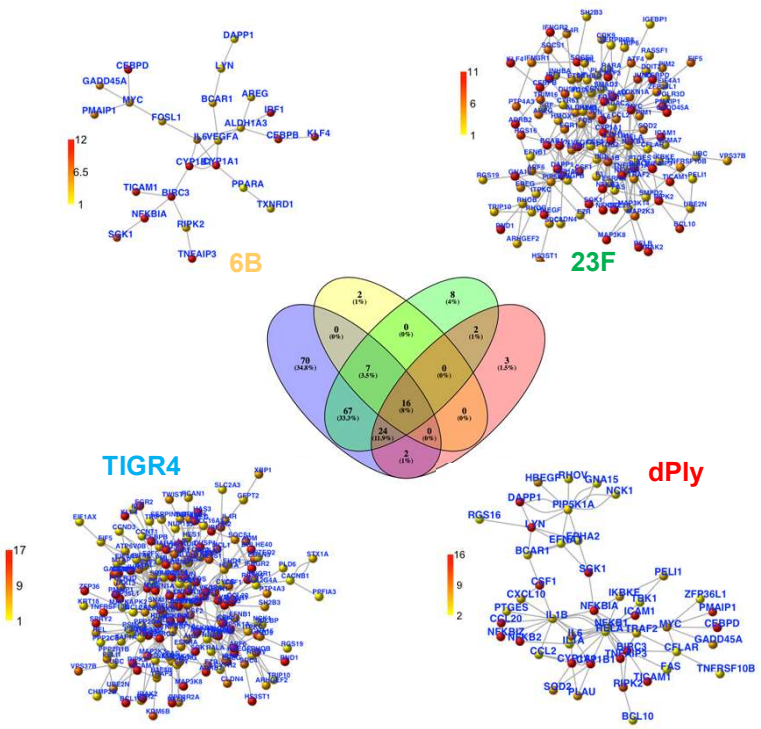
6B
23F
TIGR4
dPly

b

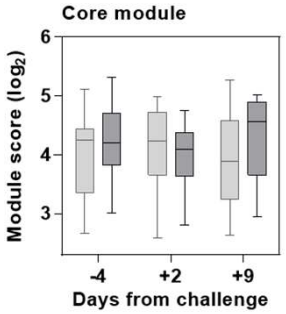
Core module
Module score (log2)
-4
+2
+9
Days from challenge

c

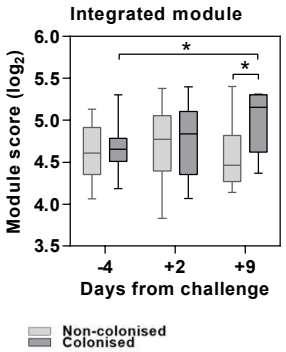
Integrated module
Module score (log2)
-4
+2
+9
Days from challenge
Non-colonised
Colonised

Figure 6

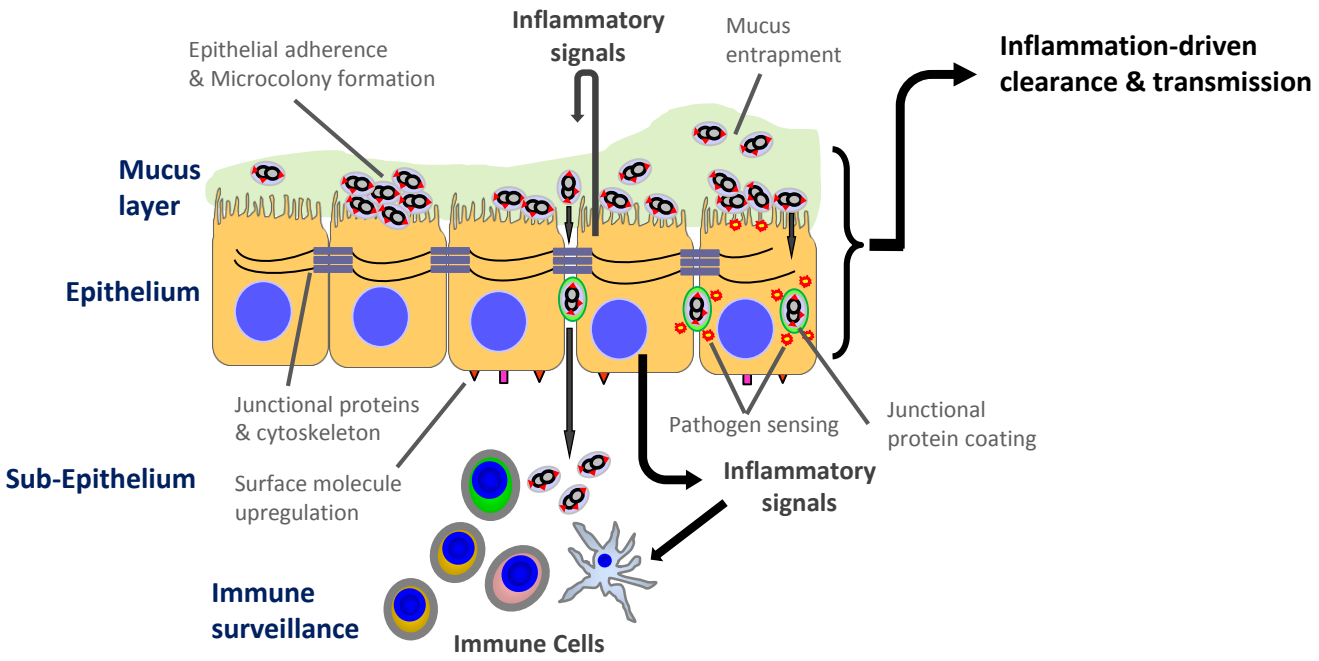
Inflammatory signals
Mucus entrapment
Epithelial adherence & Microcolony formation
Inflammation-driven clearance & transmission
Mucus layer
Epithelium
Junctional proteins & cytoskeleton
Pathogen sensing
Junctional protein coating
Sub-Epithelium
Surface molecule upregulation
Inflammatory signals
Immune surveillance
Immune Cells